CONEM 2022
CONGRESSO NACIONAL DE ENGENHARIA MECÂNICA
TERESINA - PI

ABCM

XI CONGRESSO NACIONAL DE ENGENHARIA MECÂNICA
DE 07 A 11 DE AGOSTO DE 2022, TERESINA-PI, BRASIL

TOPOLOGY OPTIMIZATION OF TUNNEL REINFORCEMENTS USING AN IBEM-FEM COUPLING MODEL

Aldemar Siqueira, a235583@dac.unicamp.br[1]
Renato Picelli, rpicelli@usp.br[2]
Josué Labaki, labaki@unicamp.br[1]

[1]School of Mechanical Engineering, University of Campinas, 200 Mendeleyev St, 13083-860, Campinas SP, Brazil
[2]Department of Mining and Petroleum Engineering, University of São Paulo, Praça Narciso de Andrade s/n, Vila Mathias, Santos - SP, 11013-560, Brazil

Abstract: *This paper considers the problem of finding optimal tunnel reinforcement distribution in the soil-structure interaction problem of a deep excavated tunnel. Topologies that result in the smallest compliance of the tunnel-soil system under prescribed restrictions for material usage are sought through the classical Bi-directional Evolutionary Structural Optimization (BESO) method. The buried tunnel is modeled via a combination of superposition of influence functions, in the sense of the Indirect Boundary Element Method (IBEM) to model the soil as an unbounded domain, together with an enclosed, optimizable portion, modeled with classical finite elements. The paper considers the cases of different in situ stresses, centered and eccentric vertical loads applied to the tunnel floor, as well as various values of reinforcement stiffness.*
Keywords: *tunnel reinforcement, topology optimization, BESO, coupled-methods, Indirect Boundary Element Method*

1. INTRODUCTION

Tunnel reinforcement is an essential technique used in tunneling engineering that aims to strengthening the surrounding ground in order to reduce the load acting over tunnel lining (Kolymbas, 2005). Various types of reinforcements can be used, such as grouts and rock bolts, generally distributed around the tunnel lining following a prescribed distribution pattern. This pattern used to be defined solely by practical experience or empirical recommendations but in the last couple of decades, following the development of topology optimization techniques, several authors addressed the optimal tunnel reinforcement problem, giving an additional tool for tunnel reinforcement design.

One of the first works in optimization of tunnel reinforcement distribution is that of Yin *et al.* (2000) who used a homogenization method to obtain the optimized distribution for a deep tunnel excavated in an elastic medium. Liu *et al.* (2008) considered the problem of minimization of tunnel heaves and used the BESO method in a fixed grid finite element framework to obtain the optimized distribution. Ghabraie *et al.* (2010) considered both shape and topology optimization of a deep tunnel profile. More recently, Nguyen *et al.* (2014) used BESO with a non-linear material model to extend previous studies and obtain a more consistent reinforcement distribution. An important common characteristic of all these works is that the soil is modeled as a large region discretized with finite elements. This initial approach is known for not being able to accurately represent the stress distribution in soil.

In this work, classical BESO algorithm is used to optimize the reinforcement distribution of a deep excavated tunnel. A small portion of soil, comprising the tunnel and its vicinity, is modeled via the Finite Element Method (FEM) and the soil is modeled as a semi-infinite elastic medium modeled by an iIndirect Boundary Element Method (IBEM) formulation. An adequate coupling scheme is presented. The effect of different *in situ* stresses, applied loads and reinforcement stiffness on the optimized reinforcement distribution are investigated.

2. PROBLEM STATEMENT

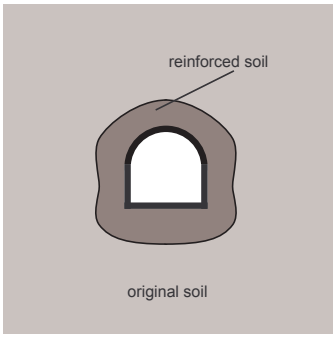

Figure 1: **Reinforced tunnel.**

Consider a deep tunnel excavated in an elastic host ground as depicted in Fig. 1. The tunnel is considered long and straight so that a plain strain case is applicable. The dark gray colored area surrounding the tunnel represents the region to be reinforced (by grouting or bolting). The problem consists in finding which is the optimal reinforcement distribution that results in the minimum tunnel deformation for a prescribed reinforcement material volume.

3. NUMERICAL MODEL

In this work, the tunnel and a small vicinity around it are modeled via a finite-boundary element coupled scheme. In this section, general details of this scheme and its application to tunnel modeling are presented.

3.1 General Soil-Structure Interaction Model

Consider a two-dimensional, isotropic, linear-elastic, arbitrarily-shaped structure of Young's modulus E_c, Poisson ratio ν_c, and mass density ρ_c, buried in a homogeneous, isotropic, linear-elastic layer with properties E_s, ν_s, ρ_s, and depth H, resting over a rigid bedrock (Fig. 2a). A rectangular-shaped domain Ω, inside the elastic layer, is modeled with classical finite elements so that an optimization scheme can easily applied (Fig. 2b). Distinct subregions within Ω may assume the material properties of the structure, denoted by the sub-index c, those of the surrounding soil medium, denoted by the sub-index s, or represent voids in the structure. The interface between Ω and the rest of the soil layer is denoted by Γ (Fig. 2c), in which $\Gamma = \Gamma_1 + \Gamma_2 + \Gamma_3 + \Gamma_4$, $\Gamma_{1,3} = (x = \pm w/2, -d - h \leq z \leq -d)$ and $\Gamma_{2,4} = (-w/2 \leq x \leq w/2, z = \{-d, -d - h\})$. Γ is discretized with piece-wise constant boundary elements, through the superposition of influence functions, in the sense of the Indirect Boundary Element Method.

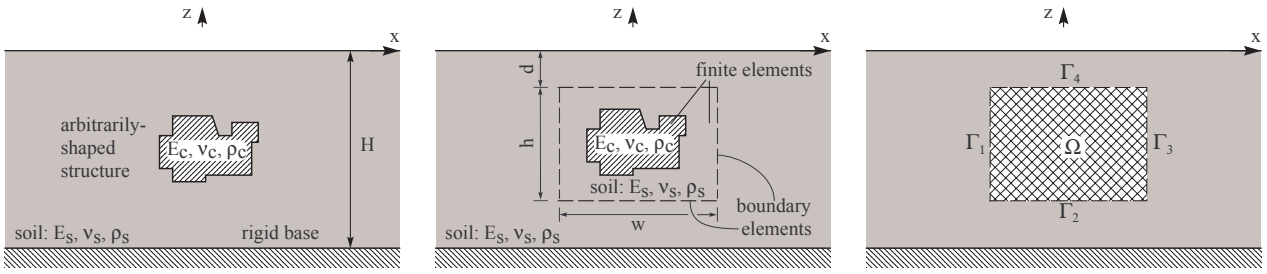

(a) (b) (c)

Figure 2: **a) arbitrarily-shaped structure buried in the soil, b) subdomains used in the finite- and boundary-element models, and c) subdomain notation.**

3.2 Model of the Structure

The domain Ω is modeled with linear-elastic, plane-strain, isoparametric quadrilateral finite elements, with four nodes and two degrees of freedom (horizontal and vertical displacements) per node. The elemental stiffness matrix is given by: $\mathbf{k}_c = \int_{-1}^{+1}\int_{-1}^{+1} \mathbf{B}^T\mathbf{C}\mathbf{B}\det[\mathbf{J}]d\xi d\eta$, where $\mathbf{B}$ is the strain-displacement transformation matrix, $\mathbf{C}$ is the constitutive matrix for the plane strain case and $\mathbf{J}$ is the Jacobian operator of the transformation between natural $(x-z)$ and parametric $(\xi-\eta)$ domains. The global stiffness matrix $\mathbf{K}_c$ of Ω is assembled from $\mathbf{k}_c$ according to the classical assembly algorithm (Bathe, 2006), and the equilibrium equation of Ω is given by

$$\mathbf{K}_c\mathbf{u}_c = \mathbf{f}_c, \tag{1}$$

in which $\mathbf{u}_c$ and $\mathbf{f}_c$ are the vector of nodal displacements and forces, respectively.

3.3 Model of the Soil Layer

In this work, an Indirect BEM is used to model the soil layer. In this framework, displacements and tractions at discrete points in the medium are related through a set of fictitious loads. In the present model, the interface Γ is discretized by $N_s = 2N_h + 2N_w$ piece-wise constant boundary elements (BE), in which N_h is the number of elements used to discretize each of the sides Γ_1 and Γ_3, and N_w is the number of elements used to discretize the bottom and top surfaces Γ_2 and Γ_4. Each element displacement and traction are measured at its center, and are given by

$$\mathbf{u}_b = \mathbf{U}\mathbf{q}, \tag{2}$$

$$\mathbf{t}_b = \mathbf{T}\mathbf{q}, \tag{3}$$

in which $\mathbf{u}_b = \left\{u_x^1\ u_z^1\ u_x^2\ u_z^2 \dots u_x^{N_s}\ u_z^{Ns}\right\}^T$ is the vector of nodal displacements, $\mathbf{t}_b = \left\{t_x^1\ t_z^1\ t_x^2\ t_z^2\ \dots t_x^{N_s}\ t_z^{Ns}\right\}^T$ is the vector of nodal tractions, $\mathbf{q} = \left\{q_x^1\ q_z^1\ q_x^2\ q_z^2 \dots q_x^{N_s}\right\}^T$ is the vector of fictitious loads, and $\mathbf{U}$ and $\mathbf{T}$ are displacement and traction influence matrices comprising the response of the soil layer. A term $u_{r,s}^{i,j}$ of matrix $\mathbf{U}$ corresponds to the displacement of an element i of the BE mesh in the r-direction due to a unit load uniformly distributed over an element j in the $s-$ direction $(i,\ j = 1, \dots, N_s;\ r, s = x, z)$. Analogously for the traction terms $t_{r,s}^{i,j}$ of matrix $\mathbf{T}$. Prescribed continuity and equilibrium conditions, respectively, for the displacements and tractions at the discrete points throughout the interface Γ must be satisfied in order to obtain the vector of unknown contact forces $\mathbf{q}$.

3.3.1 Influence Functions

Soil influence functions represent the stress and displacement fields in the soil and are written in terms of non-singular Green's functions. In this work, stress and displacement influence functions for vertically- and horizontally-distributed buried loads are used. These solutions are written in terms of improper integrals in the Fourier transformed space (Cortez *et al.*, 2022):

$$u_i(x,z) = \int_{-\infty}^{\infty} \bar{u}_i\ e^{i\zeta x} d\zeta, \tag{4}$$

$$\sigma_{ij}(x,z) = \int_{-\infty}^{\infty} \bar{\sigma}_{ij}\ e^{i\zeta x} d\zeta, \quad i,j = x,z, \tag{5}$$

where $\bar{u}_i$ and $\bar{\sigma}_i$ are functions of the elastic constants and load depth. These integrals cannot be solved analytically, thus a numerical evaluation is necessary. This task is quite difficult because their integrand contain singularities, and an oscillatory-decaying tail, which makes classical quadrature integration schemes inadequate for this task. Further discussion and details on the numerical evaluation of these integrals can be found in Cortez *et al.* (2022).

The traction influence matrix terms (Eq. (3)) are given in terms of stress influence functions by the Cauchy's formula $t_{rt}^{i,j} = \sigma_{rst}^{i,j} n_r^i$, $(r,s,t = x,z;\ i,j = 1,\dots,N_s)$, in which $\mathbf{n}^i = \left\{n_x^i\ n_z^i\right\}^T$ is the unit normal vector at the BE where the traction is being measured, pointing outward the soil domain. At Γ_1, Γ_2, Γ_3 and Γ_4, $\mathbf{n}^i = \{1\ 0\}^T$, $\mathbf{n}^i = \{0\ 1\}^T$, $\mathbf{n}^i = \{-1\ 0\}^T$ and $\mathbf{n}^i = \{0\ -1\}^T$, respectively. Influence functions for loads that are uniformly distributed in the vertical direction are used for elements placed at $\Gamma_{1,3}$ while influence functions for loads that are uniformly distributed in the horizontal direction are used for elements at $\Gamma_{2,4}$.

3.4 Structure-Soil Coupling

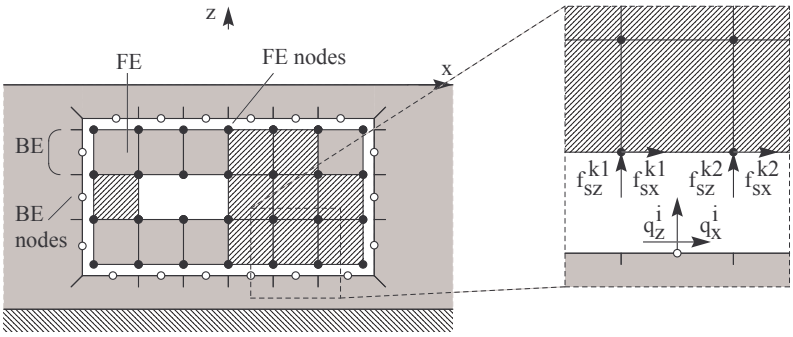

Figure 3: **Coupling.**

The present model considers an one-to-one finite-boundary element correspondence discretization of Ω and Γ. The influence of the presence of the soil in the behavior of Ω is incorporated through a set of equivalent nodal contact forces $\mathbf{f}_s$, acting at the interface nodes so that the equilibrium equation of Ω (Eq. (1)) becomes

$$\mathbf{K}_c\mathbf{u}_c = \mathbf{f}_c - \mathbf{f}_s. \tag{6}$$

At the interface, equilibrium and continuity conditions are imposed to ensure coupling between Ω and the surrounding soil. Equilibrium is obtained when the contact forces $\mathbf{q}$ acting at the soil boundary elements are fully transferred to the nodes of Ω in terms of $\mathbf{f}_s$. Since each boundary element node is associated with the two nodes of its corresponding finite element, a nodal equivalency transformation is necessary to describe the load transfer (see Fig 3). This can be obtained by $\mathbf{f}_s = \mathbf{A}\mathbf{q}$, in which $\mathbf{f}_s = \left\{ f_{sx}^1 \; f_{sz}^1 \; f_{sx}^2 \; f_{sz}^2 \ldots f_{sx}^{n_n} \; f_{sz}^{n_n} \right\}$ and $\mathbf{A}$ is a transformation matrix.

In view of this transformation, Eq. (6) can be rewritten as

$$\mathbf{K}_c\mathbf{u}_c + \mathbf{A}\mathbf{T}\mathbf{q} = \mathbf{f}_c. \tag{7}$$

Analogously, imposing the continuity condition between Ω and the rest of the soil requires a transformation between the displacements of the two nodes of each element of the finite element mesh of Ω and the displacement of the one node of their corresponding boundary element. This can be written as

$$\mathbf{u}_b = \mathbf{D}\mathbf{u}_c, \tag{8}$$

in which $\mathbf{D}$ is a transformation matrix. In view of Eq. (2) this continuity condition yields

$$\mathbf{D}\mathbf{u}_c - \mathbf{U}\mathbf{q} = \mathbf{0}. \tag{9}$$

Equations (7) and (9) can be organized into one matrix equation,

$$\begin{bmatrix} \mathbf{K} & \mathbf{A}\mathbf{T} \\ \mathbf{D} & -\mathbf{U} \end{bmatrix} \begin{Bmatrix} \mathbf{u}_c \\ \mathbf{q} \end{Bmatrix} = \begin{Bmatrix} \mathbf{f} \\ \mathbf{0} \end{Bmatrix}, \tag{10}$$

which is the equilibrium equation for nodes at the interface Γ, and

$$\begin{bmatrix} \mathbf{K} & \begin{Bmatrix} \mathbf{A}\mathbf{T} \\ \mathbf{0} \end{Bmatrix} \\ \begin{Bmatrix} \mathbf{D} & \mathbf{0} \end{Bmatrix} & -\mathbf{U} \end{bmatrix} \begin{Bmatrix} \begin{Bmatrix} \mathbf{u}_c \\ \mathbf{0} \end{Bmatrix} \\ \mathbf{q} \end{Bmatrix} = \begin{Bmatrix} \begin{Bmatrix} \mathbf{f} \\ \mathbf{0} \end{Bmatrix} \\ \mathbf{0} \end{Bmatrix}, \tag{11}$$

in which $\mathbf{0}$ are matrices of zeros of compatible dimensions. The solution of Eq. (11) for a set of prescribed external nodal forces $\mathbf{f}$ results in the nodal displacements $\mathbf{u}_c$ of Ω, as well as the set of fictitious loads $\mathbf{q}$, with which displacement and stress solutions can be computed anywhere in the soil domain.

3.5 Tunnel Design

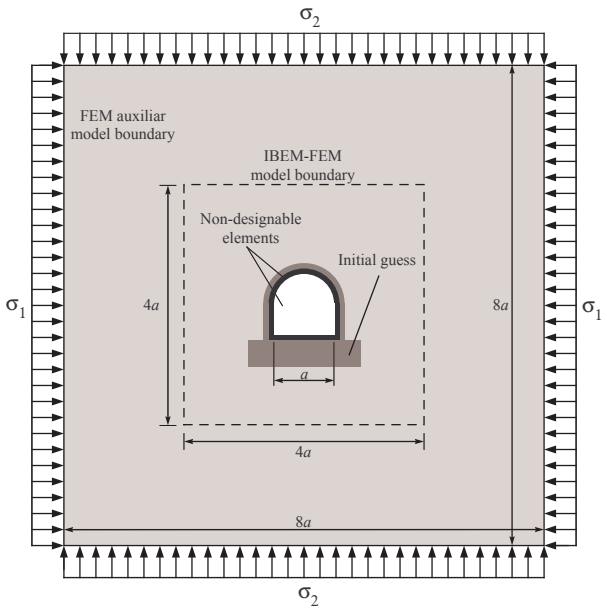

Figure 4: **IBEM-FEM model and auxiliary FEM model of tunnel excavation.**

The case of a deep tunnel is characterized by very small influence of gravity force, so that the effects of domain self-weight can be neglected (Yin and Yang, 2000) and, therefore, the pre-excavation *in situ* stresses are usually considered biaxial. Several works in tunnel design optimization model the tunnel-soil interaction solely by a finite element discretized region, which is usually large to avoid domain size effects on the results of the optimization (Yin *et al.* (2000), Nguyen *et al.* (2014)). In this work, the modeling of the soil by a boundary element formulation enables a smaller domain around the tunnel to be sufficient to represent the soil, without significant influence of the size of the domain. The present IBEM-FEM scheme is used to model a tunnel with a cross-section composed by a semi-circle of diameter a and a half-square of side length a. A square design domain of side length $4a$ is used to model the tunnel and its vicinity (Fig. 4). Since the present formulation requires an input load vector (Eq. (11)), an independent auxiliary finite element model (a square with side length of $8a$) is used to compute the effective load due to the *in situ* stresses σ_1 and σ_2. This can be achieved by restraining the displacements at nodes in the inner surface of the tunnel lining, applying the uniform biaxial stress state, computing the load response on restricted nodes, and transferring this loading as an input to the IBEM-FEM model.

Elements in the reinforced region are modeled with a larger Young's modulus than the soil. An initial guess for reinforcement distribution is considered. Elements in the tunnel excavated area are considered non-designable voids, and elements in the lining are considered as non-designable reinforcement elements.

4. TOPOLOGY OPTIMIZATION

In the present work, tunnel reinforcement optimization is considered. This problem can be stated as: given a prescribed reinforcement volume, determine the optimal reinforcement material distribution around the tunnel lining that results in the minimum tunnel deformation (Nguyen *et al.*, 2014). One way to approach this problem is by minimizing the structural compliance of an adequately selected region inside the soil (Ghabraie *et al.*, 2010), in which the tunnel and reinforcements are included. In the sense of the IBEM-FEM coupling scheme presented in Sec. (3.), this optimization problem can be written as

$$\begin{aligned} &\underset{x_i}{\text{Minimize:}}\ C(x_i) = \mathbf{f}^T \mathbf{u}_d, \\ &\text{Subject to:}\ V_r \leq \bar{V}_r, \\ &\qquad\qquad \mathbf{K}\mathbf{u}_d = \mathbf{f}, \\ &\qquad\qquad x_i \in \{0,1\},\ i \in [1, N_d], \end{aligned} \tag{12}$$

in which x_i is the vector of design variables, $C(x)$ is the structural compliance function, $\bar{V}_r$ is the specified upper bound of reinforcement material and N_d is the number of elements in the design domain. A value of $x_i = 1$ represents a reinforcement element while $x_i = 0$ represents a non-reinforcement element.

4.1 Material Interpolation Scheme

The topology design problem for the optimal distribution of multiple materials requires an adequate interpolation material scheme. For the present case, the Young's modulus of the intermediate material of an element can be expressed as (Bendsøe and Sigmund, 1999):

$$E(x_i) = x_i^p E_r + (1 - x_i^p) E_s, \tag{13}$$

where E_r is the Young's modulus of the reinforcement material and p is a penalty exponent.

4.2 Sensitivity Numbers

Sensitivity numbers represent the gradient of the objective function with respect to individual element density. Cortez *et al.* (2022) demonstrated that for a coupled IBEM-FEM structural optimization problem, similar to the present formulation, the elemental sensitivities are dependent only on the coupled structural stiffness and not on the properties of the unbounded layer. This is a direct consequence of the self-adjoint property of the structural compliance function. Consequently, elemental sensitivities can be written as (Huang and Xie, 2009)

$$\alpha_i = \begin{cases} \left[1 - \dfrac{E_s}{E_r}\right] \mathbf{u}_i{}^T \mathbf{k}_i \mathbf{u}_i, & \text{for reinforcement} \\ 0, & \text{for non-reinforcement,} \end{cases} \tag{14}$$

where $\mathbf{k}_i$ and $\mathbf{u}_i$ are the elemental stiffness matrix and the vector of nodal displacements of element i, respectively. The sensitivity numbers in Eq. (14) are obtained when the penalty factor in Eq. (13) tends to infinity.

4.3 BESO Procedure

The Bi-directional Evolutionary Structural Optimization method (BESO) procedure utilizes a sensitivity number-based rank to decide which material properties should be assumed by the elements of the domain at a given iteration. This

algorithm, presented by Huang and Xie (2007), consists of the iterative addition or removal of elements in the discretized design domain by switching the corresponding value of design variable x_i between one or zero. Firstly, a finite element analysis is performed, from which the sensitivity numbers (Eq. (14)) are computed, ranked and used as information in the addition/removal scheme. This process continues until the volume constraint given in Eq. (12) is satisfied, and from this point the volume remains constant. One can choose an initial material distribution that satisfies the volume constraint, so that the algorithm seeks to minimize the objective function by reallocating different material elements. This is the approach used in this work.

Sensitivity numbers are smoothed by a filter technique to avoid numerical instabilities such as checkerboard patterns and mesh-dependency. In this work, the filtered sensitivity number $\hat{\alpha}_i$ of element i is given by

$$\hat{\alpha}_i = \frac{\sum_{j=1}^{N_d} \alpha_i H_{ij}}{\sum_{j=1}^{N_d} H_{ij}}, \tag{15}$$

where

$$H_{ij} = \max\{0, r_f - r_{ij}\}, \tag{16}$$

in which r_f is the filter radius and r_{ij} is the distance between the centers of the i-th and j-th elements.

The sensitivity numbers of consecutive iterations are averaged in order to enhance optimization convergence properties (Huang and Xie, 2007). This can be achieved by

$$\hat{\alpha}_i^k = \frac{\hat{\alpha}_i^k + \hat{\alpha}_i^{k-1}}{2}, \tag{17}$$

where k denotes the current iteration.

When the volume constraint is satisfied, the iterative process continues until the following convergence criterion is satisfied

$$\text{error } = \frac{\left|\sum_{i=1}^{N} \left(C_{k-i+1} - C_{k-N-i+1}\right)\right|}{\sum_{i=1}^{N} C_{k-i+1}} \leq \tau, \tag{18}$$

where k is the current iteration number, τ is an allowable convergence error and N is a prescribed arbitrary integer. All examples presented in this paper consider $\tau = 10^{-4}$ and $N = 5$.

5. NUMERICAL RESULTS

In this section, the BESO algorithm combined with the present IBEM-FEM formulation are used to optimize the distribution of tunnel reinforcement. The influence of parameters such as different *in situ* stresses, application of additional loads on the tunnel floor, and different reinforcement stiffness on the optimization results is investigated. The square domain is discretized by a homogeneous mesh of 1600 finite elements and the volume of reinforcement is fixed in 20% of the domain's volume. The filter radius is considered to be twice of the element's size and a maximum number of 8 element switches per iteration is imposed to ensure that there is no abrupt changes in the optimization process. It is assumed that the reinforcement has the same Poisson's ratio $\nu_r = \nu_s = 0.25$ as the soil. All examples start from the initial reinforcement distribution shown in Fig. 4 and consider a commonly used value of reinforcement/soil stiffness ratio of $\frac{E_r}{E_s} = \frac{10}{3}$ (Yin and Yang, 2000) unless stated otherwise. Quantitative results are presented in terms of normalized structural compliance at iteration k, defined as $\bar{C}_k = \frac{C_k}{C_{k=1}}$.

5.1 Effect of in situ Stresses

The effect of the biaxial stress on the optimal reinforcement distribution is investigated for three different stress ratios $\lambda = |\sigma_1/\sigma_2|$ =0.4,1 and 1.4. Figure 5 shows the optimization results and evolution of normalized compliance of the design domain. Note that the distribution of reinforcement is strongly influenced by the *in situ* stresses and that only a few iterations are required to obtain the optimized geometry. This result is consistent with the literature and serve as a verification for the present formulation.

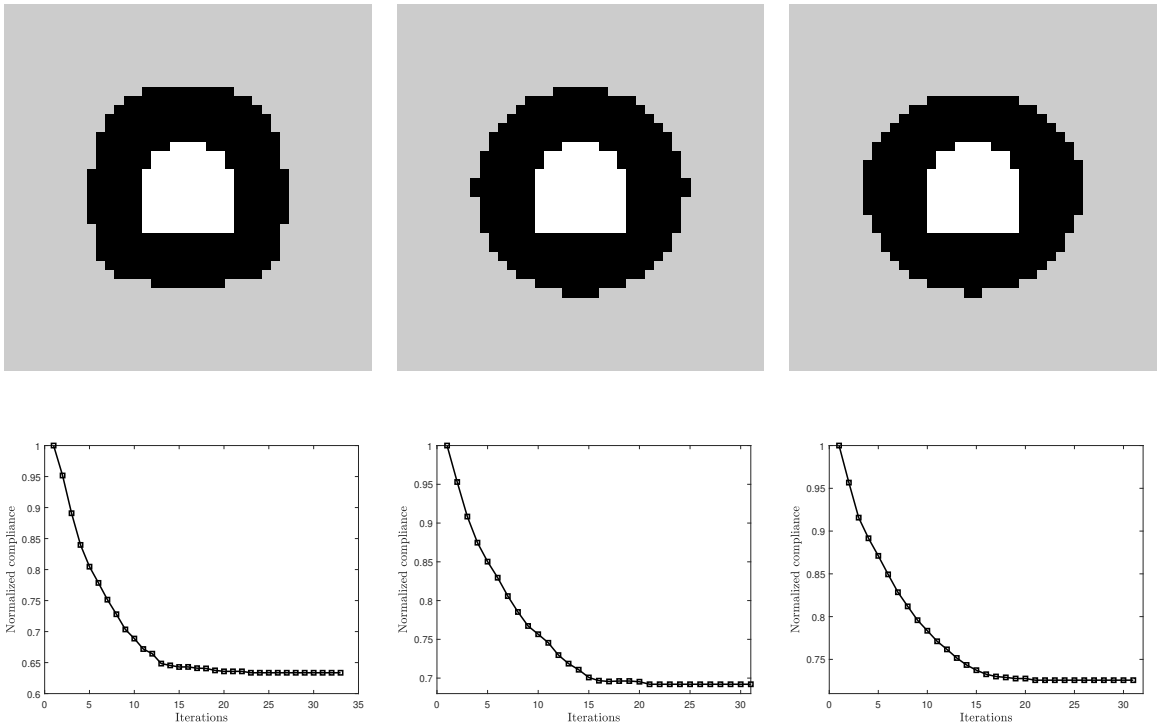

Figure 5: **The final topology and evolution of normalized compliance for a tunnel subjected to different in situ stress ratios:**$\lambda = 0.4$ **on the left,** $\lambda = 1$ **on the middle and** $\lambda = 1.4$ **on the right.**

5.2 Effect of Applied Concentrated Loads

The effect of loads applied over the tunnel floor on the optimization results is investigated for the case of concentrated centered and eccentric loads. The applied load magnitude is considered to be 40% of the total load of the soil on the tunnel's floor. Figures 6 and 7 show the final topologies obtained for three different stress ratios $\lambda = |\sigma_1/\sigma_2|$ =0.4,1 and 1.4. Note that the presence of an additional load results in reallocation of reinforcement from the lateral regions to the bottom, in order to improve stiffness in that region. When the applied load is centered, a symmetric final topology is observed, while an eccentric load results in a slightly asymmetrical topology.

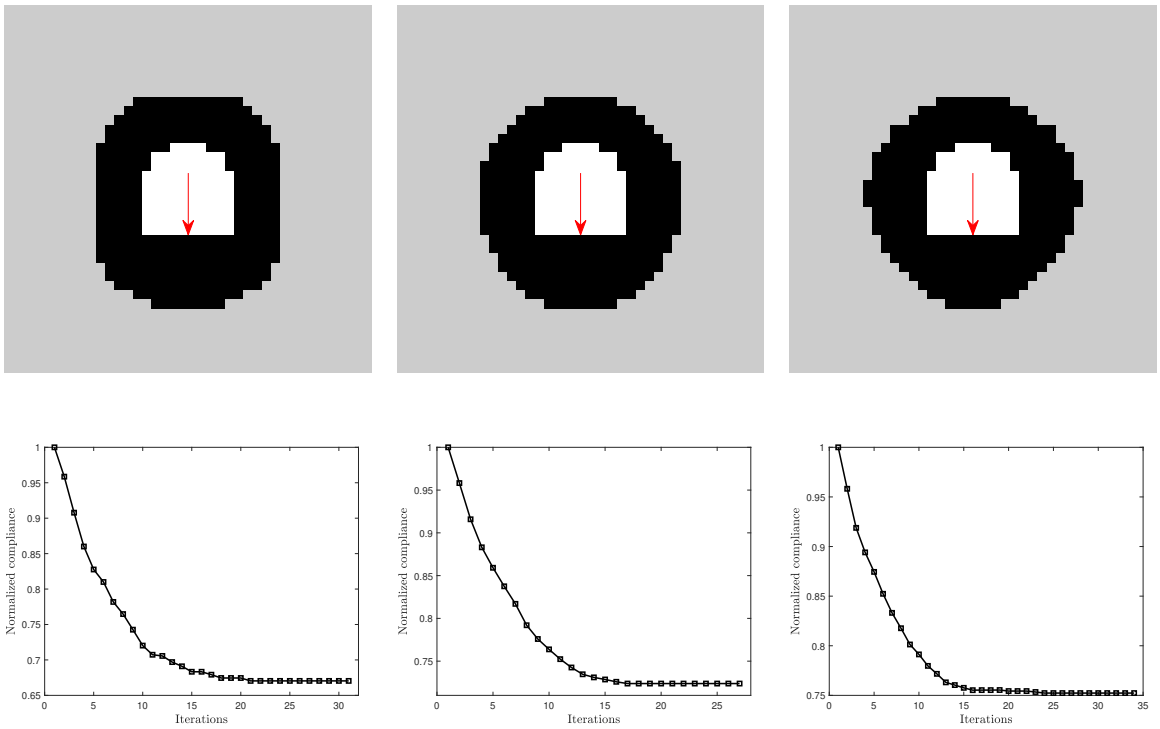

Figure 6: **The final topology and evolution of normalized compliance for a tunnel with an applied centered load:**$\lambda = 0.4$ **on the left,** $\lambda = 1$ **on the middle and** $\lambda = 1.4$ **on the right.**

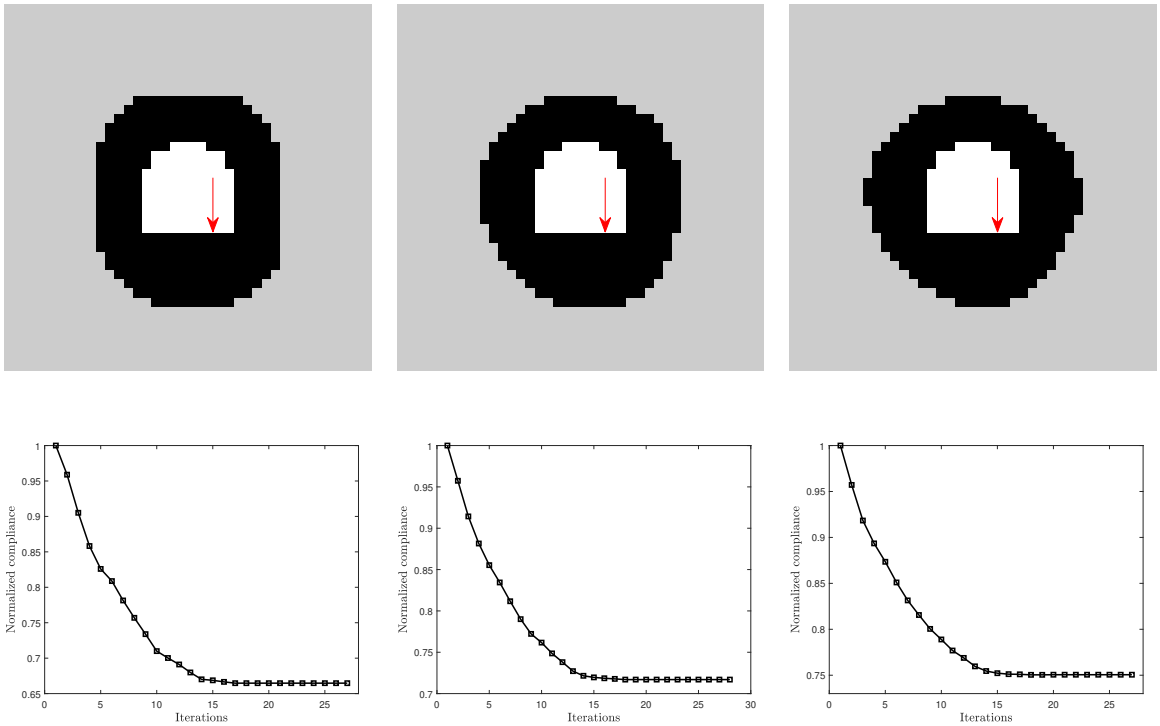

Figure 7: **The final topology and evolution of normalized compliance for a tunnel with an applied eccentric load:** $\lambda = 0.4$ **on the left,** $\lambda = 1$ **on the middle and** $\lambda = 1.4$ **on the right.**

5.3 Effect of Different Reinforcement Stiffness.

The effect of reinforcement stiffness on the reinforcement optimal distribution is investigated for a soil with stress ratio $\lambda = 1$. Figure 8 shows the final optimization results for stiffness ratios of $\frac{E_r}{E_s} = 2$ and 5. These results show that the application of stiffer reinforcements results in a more homogeneous distribution of reinforcement around the tunnel than the distribution obtained for less stiff reinforcements. For stiffness ratios larger than 5, similar results are observed.

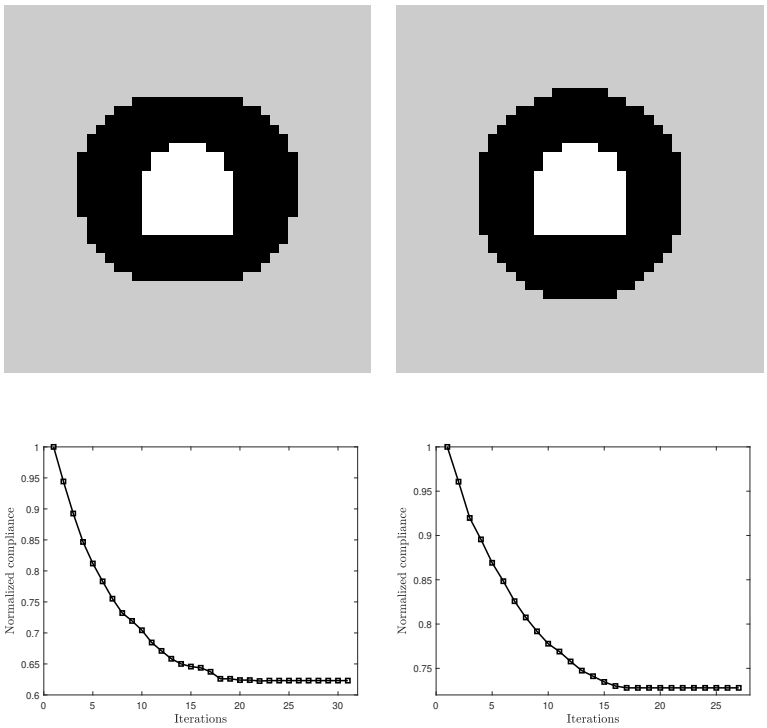

Figure 8: **The final topology and evolution of normalized compliance for a tunnel with different reinforcement stiffness:** $\frac{E_r}{E_s} = 2$ **on the left and** $\frac{E_r}{E_s} = 5$ **on the right.**

6. CONCLUSIONS

In this work, a coupled finite- boundary-element framework was used together with the classical BESO design algorithm to address the tunnel reinforcement optimization problem. The tunnel was considered to be buried deeply inside a homogeneous, semi-infinite elastic soil layer resting over a rigid bedrock. The response of the soil via computed by an Indirect-BEM formulation and was incorporated as a set of equivalent nodal loads acting over a finite-element-discretized domain comprising the tunnel region. Optimal tunnel reinforcement distribution was obtained by minimizing the structural compliance ot the domain, starting from a feasible initial reinforcement distribution. The results are consistent with the literature and indicate that *in situ* stresses, applied loads, as well as reinforcement-soil stiffness ratio have significant influence on the optimal reinforcement distribution.

7. ACKNOWLEDGEMENTS

The authors acknowledge the financial support of Brazilian National Council for Scientific and Technological Development (CNPq) through grant 132194/2021-0 and Fapesp (São Paulo Research Foundation) through grant 2018/05797-8.

8. REFERENCES

Bathe, K.J., 2006. *Finite element procedures*. Klaus-Jurgen Bathe.

Bendsøe, M.P. and Sigmund, O., 1999. "Material interpolation schemes in topology optimization". *Archive of applied mechanics*, Vol. 69, No. 9, pp. 635–654.

Cortez, R., Sivapuram, R., Barros, P., Labaki, J. and Picelli, R., 2022. "On the influence of soil flexibility in structural topology". *Computer Methods in Applied Mechanics and Engineering*. Under Review.

Ghabraie, K., Xie, Y.M., Huang, X. and Ren, G., 2010. "Shape and reinforcement optimization of underground tunnels". *Journal of Computational Science and Technology*, Vol. 4, No. 1, pp. 51–63.

Huang, X. and Xie, Y.M., 2009. "Bi-directional evolutionary topology optimization of continuum structures with one or multiple materials". *Computational Mechanics*, Vol. 43, No. 3, pp. 393–401.

Huang, X. and Xie, Y., 2007. "Convergent and mesh-independent solutions for the bi-directional evolutionary structural optimization method". *Finite elements in analysis and design*, Vol. 43, No. 14, pp. 1039–1049.

Kolymbas, D., 2005. *Tunnelling and tunnel mechanics: A rational approach to tunnelling*. Springer Science & Business Media.

Liu, Y., Jin, F., Li, Q. and Zhou, S., 2008. "A fixed-grid bidirectional evolutionary structural optimization method and its applications in tunnelling engineering". *International journal for numerical methods in engineering*, Vol. 73, No. 12, pp. 1788–1810.

Nguyen, T., Ghabraie, K. and Tran-Cong, T., 2014. "Applying bi-directional evolutionary structural optimisation method for tunnel reinforcement design considering nonlinear material behaviour". *Computers and Geotechnics*, Vol. 55, pp. 57–66.

Yin, L. and Yang, W., 2000. "Topology optimization for tunnel support in layered geological structures". *International Journal for Numerical Methods in Engineering*, Vol. 47, No. 12, pp. 1983–1996.

Yin, L., Yang, W. and Guo, T., 2000. "Tunnel reinforcement via topology optimization". *International Journal for Numerical and Analytical Methods in Geomechanics*, Vol. 24, No. 2, pp. 201–213.

9. AUTORSHIP STATEMENT

The authors are the only responsible for the printed material included in this paper.